Acta Pharmaceutica Sinica B 2022;12(4):2043–2056

Chinese Pharmaceutical Association
Institute of Materia Medica, Chinese Academy of Medical Sciences

Acta Pharmaceutica Sinica B

www.elsevier.com/locate/apsb
www.sciencedirect.com

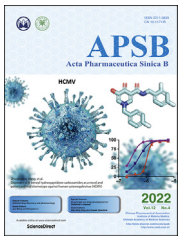

ORIGINAL ARTICLE

The effect of drug loading and multiple administration on the protein corona formation and brain delivery property of PEG-PLA nanoparticles

Yuyun Tang[a,†], Jinchao Gao[a,†], Tao Wang[b], Qian Zhang[a], Antian Wang[a], Meng Huang[a], Renhe Yu[a], Hongzhuan Chen[a,c], Xiaoling Gao[a,*]

[a]*Department of Pharmacology and Chemical Biology, Shanghai Universities Collaborative Innovation Center for Translational Medicine, Shanghai Jiao Tong University School of Medicine, Shanghai 200025, China*
[b]*Department of Geriatric Psychiatry, Shanghai Mental Health Center, Shanghai Jiao Tong University School of Medicine, Alzheimer's Disease and Related Disorder Center, Shanghai Jiao Tong University, Shanghai 200025, China*
[c]*Institute of Interdisciplinary Integrative Biomedical Research, Shuguang Hospital, Shanghai University of Traditional Chinese Medicine, Shanghai 201210, China*

Received 27 July 2021; received in revised form 23 August 2021; accepted 10 September 2021

KEY WORDS

Protein corona;
Nanoparticles;
Brain delivery;
Microglia;
PEG-PLA

Abstract The presence of protein corona on the surface of nanoparticles modulates their physiological interactions such as cellular association and targeting property. It has been shown that α-mangostin (αM)-loaded poly(ethylene glycol)-poly(L-lactide) (PEG-PLA) nanoparticles (NP-αM) specifically increased low density lipoprotein receptor (LDLR) expression in microglia and improved clearance of amyloid beta (Aβ) after multiple administration. However, how do the nanoparticles cross the blood–brain barrier and access microglia remain unknown. Here, we studied the brain delivery property of PEG-PLA nanoparticles under different conditions, finding that the nanoparticles exhibited higher brain transport efficiency

Abbreviations: αM, α-mangostin; Aβ, amyloid beta; BBB, blood–brain barrier; CNS, central nervous system; cou6, coumarin 6; cou6-NPs, cou6-labeled nanoparticles; cou7, coumarin 7; DLS, dynamic light scattering; HCS, high content screening; LDLR, low density lipoprotein receptor; MCI, mild cognitive impairment; NP, blank PEG-PLA nanoparticles; NP-αM, αM-loaded PEG-PLA nanoparticles; NP-corona complexes, nanoparticle-corona complexes; PEG-PLA, poly(ethylene glycol)–poly(L-lactide); TEER, trans-epithelial electrical resistance; TEM, transmission electronic microscope.

*Corresponding author. Tel.: +86 21 64674721.
E-mail address: shellygao1@sjtu.edu.cn (Xiaoling Gao).
[†]These authors made equal contributions to this work.

Peer review under responsibility of Chinese Pharmaceutical Association and Institute of Materia Medica, Chinese Academy of Medical Sciences.

https://doi.org/10.1016/j.apsb.2021.09.029

and microglia uptake efficiency after αM loading and multiple administration. To reveal the mechanism, we performed proteomic analysis to characterize the composition of protein corona formed under various conditions, finding that both drug loading and multiple dosing affect the composition of protein corona and subsequently influence the cellular uptake of nanoparticles in b.End3 and BV-2 cells. Complement proteins, immunoglobulins, RAB5A and CD36 were found to be enriched in the corona and associated with the process of nanoparticles uptake. Collectively, we bring a mechanistic understanding about the modulator role of protein corona on targeted drug delivery, and provide theoretical basis for engineering brain or microglia-specific targeted delivery system.

1. Introduction

The blood–brain barrier (BBB) is essential for maintaining the internal environment of the brain. However, it also largely limits the brain uptake of most pharmaceuticals[1,2], and represent a fundamental obstacle that must be overcome in the development of new treatments for brain disorder. Nanoparticulate drug delivery system is now emerging as an important means to treat the brain diseases[3,4]. However, limited amounts of nanomedicine have been reported to cross the BBB[5,6]. Therefore, the improvement of brain targeting efficiency of nanoparticles delivery systems to ensure the effectiveness of drug treatment for brain diseases is an urgent problem to be solved.

Among many polymers, PEG-PLA nanoparticles have widely been applied for drug delivery, due to its suitable safety and clinical translation ability[7–9]. Several functionalized PEG-PLA nanoparticles have been designed for brain drug delivery, with covalent conjugation of protein ligands such as lectins and the transferrin receptor antibodies on the surface of the nanoparticles[10,11]. Our previous work found that the multiple administration of αM-loaded PEG-PLA nanoparticles (NP-αM) showed a favorable biodistribution in the brain and improved the therapeutic efficacy of αM in Alzheimer's disease model mice, including reducing Aβ deposition and reversing behavioral deficits[12]. Interestingly, NP-αM specifically increased LDLR expression in microglia and enhanced the cellular uptake and degradation of Aβ[12]. However, how did the drug-loaded PEG-PLA nanoparticles cross the BBB and access microglia remain unknown, which largely hinder the optimization of the nanoformulation.

It has now been well acknowledged that when expose to biological fluids, nanoparticles attract a wide range of plasma components, resulting in the formation of protein corona[13]. Different nanoparticle physiochemical properties such as the shape, size, surface area and charge can influence the composition of protein corona[14–16]. Moreover, the corona composition varies depending on the biological environment in which nanoparticles are dispersed[13,16,17]. In contrast, the formed protein corona may play a modulatory role in the physiological interactions of the nanoparticles *in vivo*, thereby affecting the pharmacokinetics, biodistribution, cellular association, and targeting ability of nanoparticles[18,19]. Protein corona can even been utilized as a targeting strategy to direct nanoparticles into specific cells[20–22]. It is believed that any nanoparticles inevitably adsorb proteins when entering the biofluid[23]. In the case of PEGylated nanoparticle system, although PEGylation could reduce protein absorption[24], protein corona still occurs[25,26]. In addition, several literatures reported that some PEGylated nanoparticles exhibited rapid elimination upon repeated administration, with an increased accumulation in the liver and spleen[27,28]. Macrophages in the liver and spleen were speculated as the main cells to capture the nanoparticles[29]. These effects were likely due to complement proteins and anti-PEG antibodies adsorbed on the surface of nanoparticles[28,30]. Therefore, we hypothesize that drug loading and dosing frequency might change the composition of protein corona on PEG-PLA nanoparticles, and thereby affect their brain delivery property and microglia-targeted accumulation.

To test the above hypothesis, here we firstly determined and compared the brain delivery and microglia-targeting efficiency of PEG-PLA nanoparticles under different loading conditions (unloaded or αM-loaded) and dosing frequency (single dose or multiple doses). To study the role of protein corona in this process, we then prepared protein corona formed on the blank PEG-PLA nanoparticles (NP) and NP-αM by exposing them to plasma obtained from different conditions (from animal untreated or treated with the nanoparticles for 7 days) *in vitro*, and determined the cellular uptake of the nanoparticle-corona complexes (NP-corona complexes) in b.End3 (brain capillary endothelial cell line) and BV-2 microglial cells. Next, proteomics analysis was carried out to examine the composition of the corona formed on the nanoparticles. We found that the nanoparticles exhibited higher brain delivery and microglia targeting efficiency after αM loading or multiple administration. Moreover, some specific corona compositions such as complement proteins, immunoglobulins, RAB5A and CD36 were identified to be associated with nanoparticles uptake under different conditions. These different corona compositions could largely influence the brain delivery property of the nanoparticles.

2. Materials and methods

2.1. Materials and cells

Methoxy poly(ethylene glycol)$_{3000}$-poly(lactic acid)$_{40,000}$ (methoxy PEG-PLA) was kindly obtained from East China University of Science and Technology. αM was provided by Shanghai Sunny Biotech Co., Ltd. CD16/CD32 antibody (14-0161-81, Carlsbad, Invitrogen, CA, USA) and CD11b-antibody (13-0112-82, Carlsbad, Invitrogen, CA, USA) were purchased from Invitrogen. RAB5A antibody (ab66746, Cambridge, MA, USA) and CD36-antibody (ab23680, Cambridge, MA, USA) were purchased from Abcam.

Immortalized mouse brain endothelial cell line b.End3 and immortalized mouse microglial cell line BV-2 were obtained from ATCC (https://www.atcc.org/). BV-2 and b.End3 cells were cultured at 37 °C and 5% CO_2 in DMEM (SH30243.01, HyClone Laboratories Logan, UT, USA) supplemented with 10% FBS (10100147, Gibco, Carlsbad, CA, USA), 1% GlutaMAX (35050061, Thermo Fisher Scientific, Waltham, MA, USA), and 1% penicillin−streptomycin solution (15140122, Thermo Fisher Scientific, Waltham, MA, USA).

The human plasma samples were collected from subjects enrolled in the Shanghai Mental Health Center, Shanghai Jiao Tong University School of Medicine (China). The study was approved by the Institution's Ethical Committee of Shanghai Mental Health Center. Written informed consent was obtained from each study participant and/or his/her legal guardians.

2.2. Preparation and characterization of nanoparticles

Both NP and NP-αM were prepared by using the emulsion/solvent evaporation method as previously described[12]. Briefly, 10 mg methoxy PEG-PLA (to prepare NP) or 10 mg methoxy PEG-PLA and 1 mg αM (to prepare NP-αM) were dissolved in 1 mL dichloromethane, followed by the addition of 2 mL sodium cholate solution (1%, *w/v*). Then the solution was emulsified by probe sonication (220 W, 2 min) on ice to form oil-in-water emulsion. After that, the resulting emulsion was magnetically stirred in 18 mL sodium cholate solution (0.5%, *w/v*) for 5 min. The RE-2000A rotary vacuum evaporator (RE-2000A, Yarong, Shanghai, China) was employed to evaporate the dichloromethane. Then the nanoparticles were obtained by centrifugation at 18,000×*g* for 45 min (Multifuge X1R, Thermo Fisher Scientific, Waltham, MA, USA).

Fluorescent-labeled NP/NP-αM were prepared through the similar process above with coumarin 6 (cou6) as the fluorescent probe. First, 10 mg methoxy PEG-PLA and 0.1 mg cou6 (to prepare cou6-labled NP) or 10 mg methoxy PEG-PLA, 1 mg αM and 0.1 mg cou6 (to prepare cou6-labled NP-αM) were dissolved in 1 mL dichloromethane. The next steps were performed with the same procedure of NP/NP-αM preparation. The unentrapped cou6/αM was removed with the application of a sepharose CL-4B column.

The zeta potential and particle size of nanoparticles were measured using a dynamic light scattering (DLS, Zetasizer Nano-ZS90, Malvern, UK) detector. The morphology of nanoparticles was characterized with a JEM-1400 plus transmission electronic microscope (JEM-1400 plus TEM, JEOL, Tokyo, Japan). Samples were negatively stained with a 2% solution of sodium phosphotungstate. The function groups on the surface of NP and NP-αM were determined *via* ^{1}H NMR analysis (Thermo Fisher Scientific, Waltham, MA, USA) after dissolving in DMSO-d_6.

2.3. Drug-loading capacity (DLC) and encapsulation efficiency (EE) of NP-αM

NP-αM were dissolved in acetonitrile for 5 min, then the supernatant was collected. The concentration of αM in NP-αM was determined by HPLC with a Venusil MP C18 column (5 μm, 4.6 mm × 150 mm, Agela Technology, Tianjin, China). The mobile phase was consisted of methanol and 5 mmol/L ammonium formate buffer (pH 3.0, 94:6) with 1.0 mL/min flow rate. The wavelength of ultraviolet detector was 325 nm.

The DLC of NP-αM was calculated as shown in Eq. (1):

$$\mathrm{DLC}\ (\%) = \frac{C_1 \times N}{C_2} \times 100 \quad (1)$$

The EE of NP-αM was calculated as shown in Eq. (2):

$$\mathrm{EE}\ (\%) = \frac{C_1 \times N \times M_2}{M_1 \times C_2} \times 100 \quad (2)$$

C_1 is the detected concentration of αM, C_2 is the concentration of nanoparticle solution, N is the dilution factor, M_1 is the dosage of αM, and M_2 is the dosage of PEG-PLA compound.

2.4. Animals and treatments

Three-months old female C57BL/6 mice were provided by Shanghai SLAC Laboratory Animal Co., Ltd., maintained in pathogen-free condition with controlled humidity and temperature. The animal experiments were performed according to the institutional guidelines from Shanghai Jiao Tong University School of Medicine (China).

The mice were divided into four administration groups. For the 0d-NP and 0d-NP-αM groups, the mice were intravenously administered with the cou6-labeled NP and NP-αM in a single-dose (70 mg/kg nanoparticles, containing 0.2 mg/kg cou6), respectively. For the 7d-NP and 7d-NP-αM groups, the mice were intravenously administered with NP and NP-αM for 6 days, respectively, and the cou6-labeled NP or NP-αM were administered at the last day (70 mg/kg, containing 0.2 mg/kg cou6). At the designed time points (20, 60 and 100 min) post-administration, the mice (n = 3−5 per time point for each groups) were anesthetized with ketamine (100 mg/kg) and xylazine (10 mg/kg) through intraperitoneal administration. The blood was harvested, and the brains were collected after cardiac perfusion with saline. The brain samples were then weighed for the quantitative analysis of the cou6-labeled nanoparticles (cou6-NPs).

2.5. Isolation of primary microglial cells

Primary microglial cells were obtained from C57/BL6 mice by using magnetic beads according to the manufacturer's protocol (11047, Dynabeads Biotin Binder, Invitrogen, Carlsbad, CA, USA). The mice were sacrificed at 60 min after administration with the brain tissues collected. Then the brains were cut into fine pieces in DMEM supplement with 1% GlutaMAX and 1% penicillin−streptomycin solution. The resulting single-cell suspension was prepared by enzymatic dissociation with 200 U/mL papain enzyme for 15 min at 37 °C. After that, the cells were incubated with 100 μL anti-CD11b pre-conjugated magnetic beads for 30 min at 4 °C, and then placed on a magnetic holder for 2 min for removing the supernatant containing the unbound cells. After that, the cells were added with 4 mL of isolation buffer and washed for four times to achieve high purity.

2.6. Detection of cou6

The level of cou6 in the mice blood, brain, and microglia were analyzed using high performance liquid chromatography (HPLC, Shimadzu, Japan). Briefly, cou6 were released from microglial cells upon repeated freezing and thawing. The resulting cell splitting solution, brain homogenate and blood were extracted by the addition of hexane with coumarin 7 (cou7) as the internal standard. After vortexing for 2 min, the mixture was centrifuged at 18,000×*g* for 5 min (Multifuge X1R, Thermo Fisher Scientific).

After that, the supernatant was collected and vaporized under a vacuum concentrator, followed by redissolving in methanol and consequence centrifuging at 18,000×*g* for 5 min. The supernatant was collected and then measured by HPLC with a Venusil MP C18 column (5 μm, 4.6 mm × 150 mm, Agela Technology, Tianjin, China). The mobile phase was consisted of methanol and water (96:4) with 1.0 mL/min flow rate and 35 °C column temperature. The excitation and emission wavelength were 465 and 502 nm, respectively.

The brain/blood ratio of cou6 was calculated as shown in Eq. (3):

$$\text{Brain}\,/\,\text{blood ratio} = \frac{\text{Amount of cou6 in brain}}{\text{Amount of cou6 in blood}} \quad (3)$$

Brain tissue samples and the splitting solution of microglial cells were normalized by levels of total proteins detected by BCA Protein Assay. The microglia/brain ratio of cou6 was calculated as shown in Eq. (4):

$$\text{Microglia}\,/\,\text{brain ratio} = \frac{\frac{\text{Amount of cou6 in microglia}}{\text{Total protein content of microglia}}}{\frac{\text{Amount of cou6 in brain}}{\text{Total protein content of brain}}} \quad (4)$$

2.7. Preparation of the NP-corona complexes

NP or NP-αM were administered intravenously (70 mg/kg) in C57/BL6 mice for 7 days. Twenty-four hours post-injection, the blood was collected in tubes with heparin anticoagulation. Blood from the untreated mice was also collected. 7d-plasma (from animal treated with nanoparticles for 7 days) and 0d-plasma (from animal untreated) were then prepared by centrifugation at 1200×*g* at 4 °C for 10 min (Multifuge X1R, Thermo Fisher Scientific). Immediately after that, NP and NP-αM (300 μL, 10 mg/mL) were incubated with 0d-plasma and 7d-plasma (150 μL) for 1 h at 37 °C, respectively. Following the incubation, the samples were centrifugated at 18,000×*g* (Multifuge X1R, Thermo Fisher Scientific), 4 °C for 10 min and washed two times with PBS. Based on the nanoparticle loading (unloaded or αM-loaded) and incubation conditions (0d-plasma or 7d-plasma), either 0d-NP-corona, 7d-NP-corona, 0d-NP-αM-corona or 7d-NP-αM-corona was obtained. The resulting NP-corona complexes were redissolved in PBS with the zeta potential and particle size detected with DLS, and the morphology characterized *via* TEM analysis following negatively staining with a 2% solution of sodium phosphotungstate.

2.8. Mass spectrometry analysis

Three replicates of NP-corona complexes (0d-NP-corona, 7d-NP-corona, 0d-NP-αM-corona, 7d-NP-αM-corona) were prepared. Protein corona was eluted from nanoparticles by incubation in 2% SDS for 10 min at 100 °C, followed by centrifugation at 18,000×*g* for 10 min. The supernatant was collected and the protein concentration was detected by BCA Protein Assay. The samples were reduced in the addition of 10 mmol/L dithiothreitol at 37 °C for 1 h, followed by alkylation with 55 mmol/L iodoacetamide for 1 h in dark. The proteins were then exchanged with NH_4HCO_3 (50 mmol/L) and centrifugation for 20 min at 14,000×*g* for 3 times. After digesting with trypsin, the samples were centrifugated at 14,000×*g* for 20 min. The resulting tryptic peptides were subsequently incubated with 1% trifluoroacetic acid (TFA). C18 Ziptips was employed to purified the samples in 0.1% TFA with 50% acetonitrile. After lyophilizing *via* a SpeedVacuum (ThermoSavant, Thermo Fisher Scientific, Waltham, MA, USA) for 2 h, the samples were redissolving in 1% formic acid with 5% acetonitrile.

Afterward, data-dependent acquisition (DDA) analysis for library generation were performed on an Orbitrap Exploris 480 mass spectrometer connected to an Easy-nLC 1200 chromatography system *via* an Easy Spray (Thermo Fisher Scientific). Samples were separated with a self-packed analytical PicoFrit column (75 μm × 40 cm, New Objective) packed with ReproSil-Pur 120 C18-AQ (1.9 μm, Dr. Maisch GmbH, Germany). The DDA raw data were matched with the mouse Uniprot fasta database using the Pulsar search engine (available in Spectronaut Pulsar). Each sample was analyzed in a data-independent acquisition (DIA) mode and the raw files were analyzed in Spectronaut X (Biognosys, Switzerland). The false discovery rate (FDR) was set to 1% for analysis.

The composition of 0d-plasma, 7d-plasma ($n = 4$ for each group), and protein corona formed on NP-αM incubated with plasma from mild cognitive impairment (MCI) patients (MCI-NP-αM-corona) and healthy people (Healthy-NP-αM-corona) ($n = 5$ for each group) were also determined *via* the same method.

2.9. Qualitative and quantitative analysis of the cellular uptake of cou6-NPs

BV-2 or b.End3 cells were seeded into 24-well glass-bottom plates at 50,000 cells/well and cultured overnight. Then the cells were incubated with cou6-labeled NP, NP-αM, 0d-NP-corona, 7d-NP-corona, 0d-NP-αM-corona, or 7d-NP-αM-corona at the concentration of 15 μg/mL in DMEM at 37 °C for 3 h. After washing with PBS, the cells were fixed with 3.7% formaldehyde for 10 min and triple rinsed with PBS. Then the cells were stained with DAPI for 10 min and qualitatively analyzed by confocal microscope (Leica TCS SP8, Weztlar, Germany).

Quantitative analysis of the cellular uptake of the six cou6-NPs was measured through a high content screening (HCS) reader (CX5 HCS, Thermo Fisher Scientific, Waltham, MA, USA). BV-2 or b.End3 cells were seeded into 96-well plates at 5000 cells/well. After cultured overnight, the cells were incubated with 15 μg/mL cou6-NPs in DMEM at 37 °C for 3 h, and, then fixed and qualitatively analyzed using HCS.

2.10. Permeability of NP-corona complexes across the BBB model

To build up a simple BBB model, b.End3 cells were seeded into a Transwell insert (PIRP12R48, Millipore, Billerica, MA, USA) pre-coated with collagen I at 10^5 cells/cm^2. The tight junction protein claudin-5 in the BBB model was detected under a laser confocal microscope. The trans-epithelial electrical resistance (TEER) were measured at the culture time of 2, 4 and 6 days. Permeability study were performed when TEER became consistent. The cou6-labeled NP-corona complexes were added to the upper chamber in DMEM. The medium in the lower chamber were collected at the designed time points (1, 2, 4, 8 and 24 h). The nanoparticles concentrations were determined through fluorescence quantification using a multimode microplate reader (Varioskan™ LUX, Thermo Fisher Scientific, Waltham, MA, USA).

To evaluate cellular uptake of NP-corona complexes in BV-2 cells in the BBB model. BV-2 cells were seeded into the lower chamber at 50,000 cells/well and cultured overnight. The cellular

uptake of NP-corona complexes in BV-2 cells at 12 h were qualitatively analyzed using HCS and qualitatively analyzed by confocal microscope (Leica TCS SP8).

2.11. *Mechanisms of the cellular uptake of the cou6-NP-corona complexes*

To study the mechanisms of the cellular uptake of the different NP-corona complexes, BV-2 or b.End3 cells were seeded into 96-well glass-bottom plates at 5000 cells/well, and cultured overnight. To study the involvement of CD16/32, the cells were pre-incubated with 5 μg/mL anti-CD16/32 for 24 h. To reveal the function of complement protein, ethylene diamine tetraacetic acid (EDTA) treatment was performed to inhibit the binding of complement protein to the surface of nanoparticles, in which the nanoparticles were incubated with the plasma in the presence of 10 mmol/L EDTA. To determine the involvement of RAB5A or CD36, NP-corona complexes were incubated with RAB5A or CD36 antibody (1 μg/mL) for 1 h to block RAB5A or CD36 in the corona. After that, the NP-corona complexes were incubated with cells in serum-free DMEM at the concentration of 15 μg/mL at 37 °C for 3 h, and then the cells were fixed and qualitatively analyzed using HCS.

2.12. *Statistical analysis*

All data were analyzed with GraphPad Prism software and expressed as mean ± SD unless otherwise indicated. Two-tailed Student's *t*-test was used for two-group comparison. One-way ANOVA was used for multiple-group comparison. Differences were considered to be statistically significant at $P < 0.05$.

3. Results

3.1. *Multiple-dose or αM-loaded PEG-PLA nanoparticles show higher brain distribution and microglial accumulation*

NP and NP-αM were prepared by means of ultrasonic emulsification as described previously. The DLC of NP-αM was 2.71 ± 0.12% with the EE 43.3 ± 5.1%. The size of NP and NP-αM were 85.1 ± 6.2 and 147.8 ± 5.6 nm, and their zeta potential were −21.1 ± 1.7 and −20.6 ± 0.8 mV, respectively. Their size and zeta potential hardly changed after labeling with cou6 (Supporting Information Table S1), a widely-used probe for PEG-PLA nanoparticles, which can be well reserved in the nanoparticles and largely represent their behavior[31−33].

To evaluate the brain delivery property of PEG-PLA nanoparticles under different dosing frequency or loading conditions, we injected single-dose (0d) or multiple-dose (7d) of NP or NP-αM into C57/BL6 mice, respectively. Then we collected blood and brain, and isolated microglial cells by using magnetic beads. The amounts of cou6-NPs were determined by HPLC, and the protein content of brain and microglia was determined by BCA Protein Assay (Fig. 1A). 0d-NP, 7d-NP, 0d-NP-αM and 7d-NP-αM exhibited very similar pharmacokinetic profiles in blood, that is, similar area under the blood concentration−time curve (AUC_{all}) were achieved (Fig. 1B, Supporting Information Table S2). Intriguingly, biodistribution analysis showed that, compared with NP, NP-αM achieved an improved brain biodistribution profile with the AUC_{all} of cou6-NPs in brain enhanced by 2.35- and 1.91-fold for the single-dose and multiple-dose group, respectively (Fig. 1C, Supporting Information Table S3).

We next evaluated the brain/blood ratio of cou6-NPs at 60 min (Fig. 1D, Supporting Information Tables S4 and S5). Compared with that of 0d-NP-αM, the brain/blood ratio of 7d-NP-αM was enhanced by 79%. Similarly, the brain/blood ratio of 7d-NP was increased by 83% compared with 0d-NP (Fig. 1D). This suggested that nanoparticles with multiple-dose exhibited higher brain/blood ratio than that with single-dose in mice. In addition, the brain/blood ratio presented a dramatically enhancement in the αM-loaded nanoparticles compared with unloaded ones. 7d-NP-αM exhibited 2.3-fold higher brain distribution than 7d-NP. Consistently, 0d-NP-αM showed 2.2-fold higher brain distribution than 0d-NP (Fig. 1D). Also, the AUC_{brain}/AUC_{blood} ratio of 7d-NP-αM (1.69) were found to be much higher than that of 7d-NP (0.43), and 0d-NP-αM (1.40) also showed a significant enhancement in AUC_{brain}/AUC_{blood} ratio when compared with 0d-NP (0.38) (Tables S2 and S3). Together, these results suggest that after multiple administration or αM loading, PEG-PLA nanoparticles showed higher brain transport efficiency.

To study the effect of loading condition and dosing frequency on microglia uptake efficiency, we determined the microglia/brain ratio of cou6-NPs at 60 min. It was found that PEG-PLA nanoparticles with multiple-dose exhibited much higher brain/blood ratio than that with single-dose in mice. The microglia/brain ratio of 7d-NP-αM was increased by 68% compared with that of 0d-NP-αM, while that of 7d-NP was enhanced by 62% compared with that of 0d-NP. Besides, αM-loaded nanoparticles showed higher microglia/brain ratio than the unloaded ones. The microglia/brain ratio of 7d-NP-αM was elevated by 78% compared with that of 7d-NP, while that of 0d-NP-αM was enhanced by 76% compared with that of 0d-NP (Fig. 1E).

The above data indicated that, both drug loading and dosing frequency exert great influence on the brain delivery property the PEG-PLA nanoparticles. Compared with single-dose, PEG-PLA nanoparticles with multiple-dose exhibited higher brain transport efficiency and microglia uptake efficiency. αM-loaded nanoparticles showed the same result compared with unloaded. Upon exposure to biofluid, nanoparticles adsorb a multitude of proteins. It is believed that the composition of this protein corona is depend on the physiochemical properties of nanoparticles and the biological environment[34−36], thereby providing the nanoparticles with a "biological" identity that influences physiological interactions *in vivo*[13]. We hypothesized that different coronas formed on nanoparticles affect the brain delivery *via* different mechanisms to enter the cells.

3.2. *Preparation and characterizations of the NP-corona complexes*

In order to prepare different NP-corona complexes and study the effect of corona on cellular uptake mechanisms, the nanoparticles were incubated in different plasma of C57 mice *in vitro*. We prepared protein corona formed on NP and NP-αM by exposing them to plasma obtained from 0d-plasma (from animal untreated) or 7d-plasma (from animal treated with the nanoparticles for 7 days) to mimic single-dose or multiple-dose of nanoparticles *in vivo*. Based on the nanoparticle loading (unloaded or αM-loaded) and incubation conditions (0d-plasma or 7d-plasma), either a 0d-NP-corona, 7d-NP-corona, 0d-NP-αM-corona or 7d-NP-αM-corona was obtained (Fig. 2A).

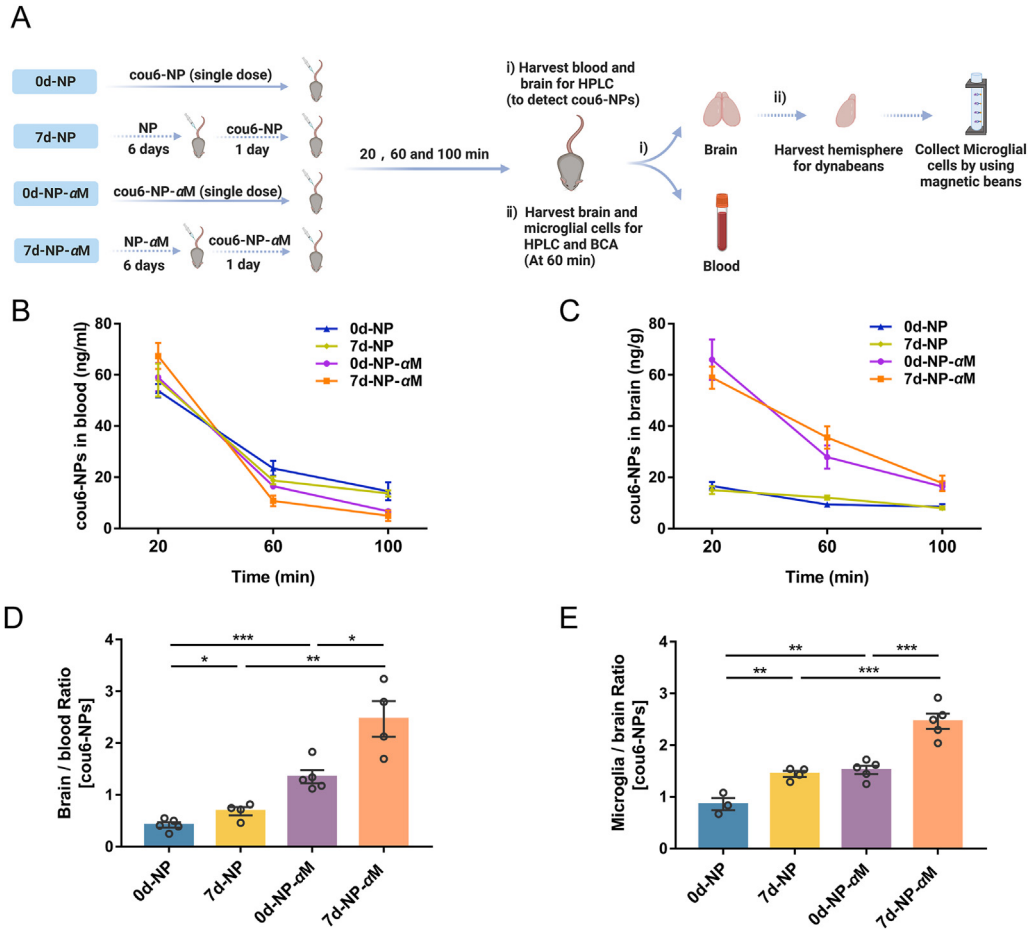

Figure 1 Brain distribution of PEG-PLA nanoparticles under different loading condition and dosing frequency. (A) Schematic of the nanoparticles administered into C57/BL6 mice (70 mg/kg, i.v.). Microglial cells were isolated by using magnetic beads. The concentration of cou6-NPs in blood, brain and microglial cells was determined by HPLC. The protein content of brain and microglial cells was determined by BCA Protein Assay. (B and C) The concentrations of cou6-NPs in blood (B) and brain (C) at 20, 60 and 100 min after administration. (D) Brain/blood ratio of cou6-NPs at 60 min. (E) The ratio of cou6-NPs in microglial cells and brain tissue at 60 min. The microglial cells and brain tissue were normalized by levels of total proteins detected by BCA. $n = 3-5$ per time point for each groups. Data are presented as the mean ± SEM. $^{*}P < 0.05$, $^{**}P < 0.01$, $^{***}P < 0.001$, $^{****}P < 0.0001$.

TEM visualized the protein corona on the surface of the NP-corona complexes (Fig. 2B and C). αM loading significant increase the size of nanoparticles. Moreover, NP-corona complexes showed a bigger size compared to that without corona (Fig. 2B–D). In contrast, the zeta potentials of nanoparticles were all negative and hardly changed following the formation of protein corona (NP −21.4 ± 0.9 mV, 0d-NP-corona −19.0 ± 0.6 mV, 7d-NP-corona −20.0 ± 0.6 mV, NP-αM −20.5 ± 0.6 mV, 0d-NP-αM-corona −22.0 ± 1.3 mV, and 7d-NP-αM-corona −20.2 ± 0.5 mV, Fig. 1E).

3.3. *Cellular uptake of NP-corona complexes*

To examine the cellular uptake efficiency of NP-corona complexes *in vitro*, b.End3 and BV-2 cells were used as cell models correspond to the situation of brain and microglial cells delivery respectively. Quantitative analysis showed that NP-corona complexes (7d-NP-corona or 7d-NP-αM-corona) displayed significant higher cellular uptake in b.End3 and BV-2 cells compared to nanoparticles without corona (NP or NP-αM, Fig. 3A and C). In addition, the uptake of NP-corona complexes incubated with 7d-plasma (7d-NP-corona or 7d-NP-αM-corona) was much higher than that with 0d-plasma (0d-NP-corona or 0d-NP-αM-corona). In addition, compared with that unloaded (0d-NP-corona or 7d-NP-corona), αM-loaded NP-corona complexes (0d-NP-αM-corona or 7d-NP-αM-corona) showed a significant enhancement in cellular uptake (Fig. 3A and C). Such findings were confirmed by confocal imaging analysis (Fig. 3B and D).

In the absence of protein corona, NP-αM also exhibited an increased cell uptake compared with NP. ^{1}H NMR spectrum shows a significant difference in the third peak ($\delta = 3.4$) between NP and NP-αM (Supporting Information Figs. S1 and S2), which could be derived from the methoxy group (CH_3O–) of αM. The increased hydrophobic functional group CH_3O– on the surface of NP-αM could be a possible reason that αM loading promote the cellular uptake of nanoparticles.

Furthermore, we investigated the ability of NP-corona complexes to cross the BBB by using b.End3 cells monolayer as an *in vitro* BBB model (Fig. 4A) as described previously[37]. The trans-epithelial electrical resistance (TEER) reached 172 Ω·cm^2 and the expression of tight junction protein claudin-5 was well observed when the cells were cultured for 6 days (Fig. 4B and C). NP-corona complexes

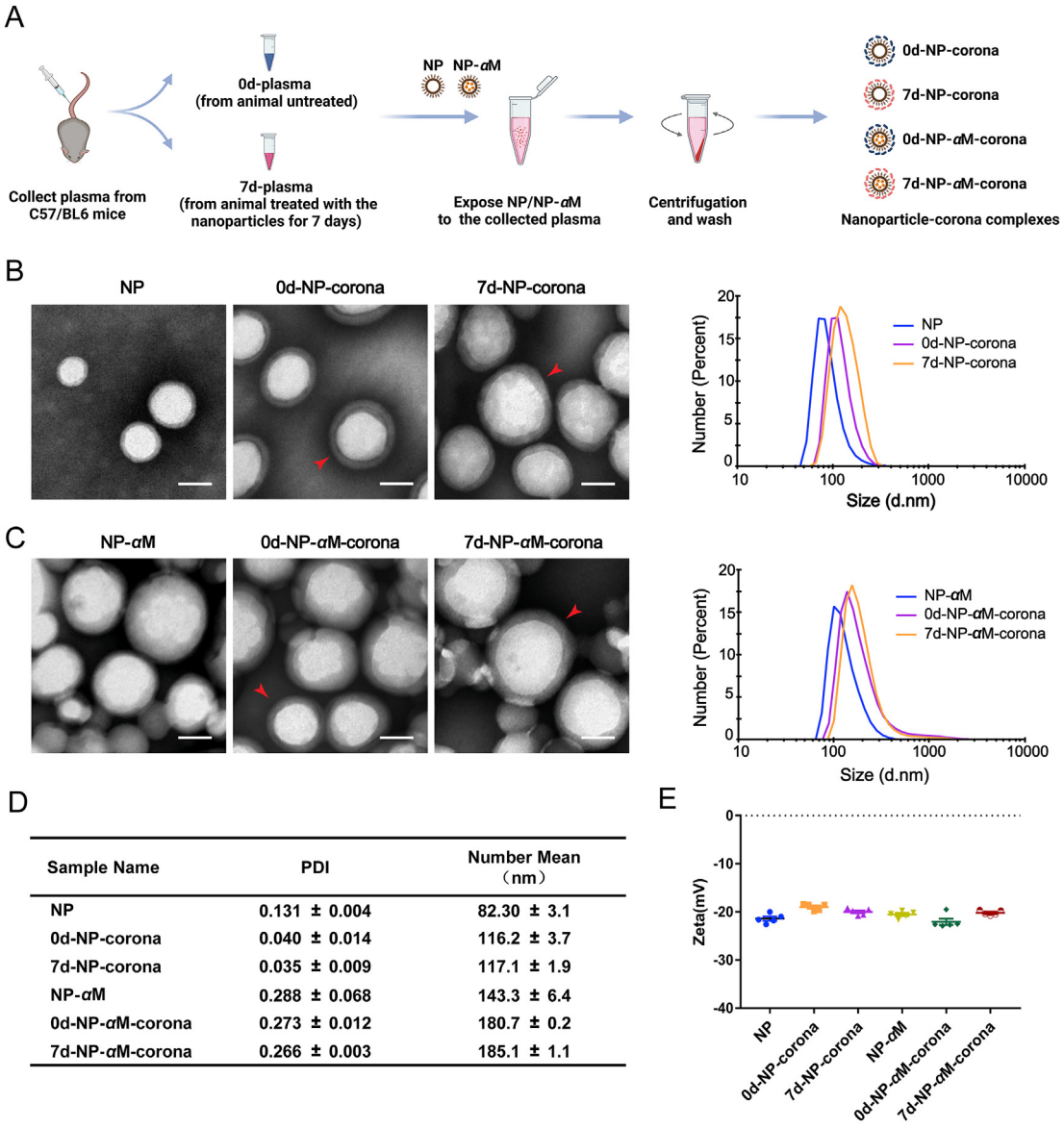

Sample Name	PDI	Number Mean (nm)
NP	0.131 ± 0.004	82.30 ± 3.1
0d-NP-corona	0.040 ± 0.014	116.2 ± 3.7
7d-NP-corona	0.035 ± 0.009	117.1 ± 1.9
NP-αM	0.288 ± 0.068	143.3 ± 6.4
0d-NP-αM-corona	0.273 ± 0.012	180.7 ± 0.2
7d-NP-αM-corona	0.266 ± 0.003	185.1 ± 1.1

Figure 2 Preparation and characterizations of the corona formed on NP and NP-αM in 0d-plasma or 7d-plasma. (A) Schematic illustration of the NP-corona complexes preparation setup: the NP and NP-αM were incubated with plasma from untreated C57 mice or animal treated with the nanoparticles for 7 days. (B and C) Morphology and particle size distribution of NP/0d-NP-corona/7d-NP-corona (B) and NP-αM/0d-NP-αM-corona/7d-NP-αM-corona (C) under TEM and DLS. Scale bar = 50 nm. (D) Particle size and PDI of the nanoparticles (n = 5). (E) Zeta potential of the nanoparticles (n = 5).

with αM loading (0d-NP-αM-corona or 7d-NP-αM-corona) resulted in a significant higher percentage transport compared with that unloaded (0d-NP-corona or 7d-NP-corona). And the transport of NP-corona complexes formed in 7d-plasma (7d-NP-corona or 7d-NP-αM-corona) was much higher than that formed in 0d-plasma (0d-NP-corona or 0d-NP-αM-corona, Fig. 4D). Such findings are in accordance with that found in nanoparticles uptake by bEnd.3 cells (Fig. 3A and B) and the brain transport efficiency *in vivo* (Fig. 1D).

To better reflect the interaction between the nanoparticles and microglia, the cellular uptake of nanoparticles was evaluated by culturing BV-2 cells at the bottom of the BBB model, in which the nanoparticles should firstly cross the BBB and then get access to the microglia (Fig. 4A). Similarly, the BV-2 uptake showed a dramatically enhancement in NP-corona complexes with αM loading (0d-NP-αM-corona or 7d-NP-αM-corona) compared to unloaded (0d-NP-corona or 7d-NP-corona). The uptake of NP-corona complexes formed in 7d-plasma (7d-NP-corona or 7d-NP-αM-corona) was also much higher than that formed in 0d-plasma (0d-NP-corona or 0d-NP-αM-corona, Fig. 4E and F). Such findings are also in accordance with that found in nanoparticles uptake by BV-2 cells (Fig. 3C and D) and the microglia uptake efficiency *in vivo* (Fig. 1E).

3.4. *Proteomics analysis of the protein corona*

Under different loading and incubation, the composition of these protein coronas formed on nanoparticles conditions may varied a lot, which may contribute to the differences in cellular uptake. To examine the composition of the corona formed on nanoparticles, proteomics analysis was carried out using mass

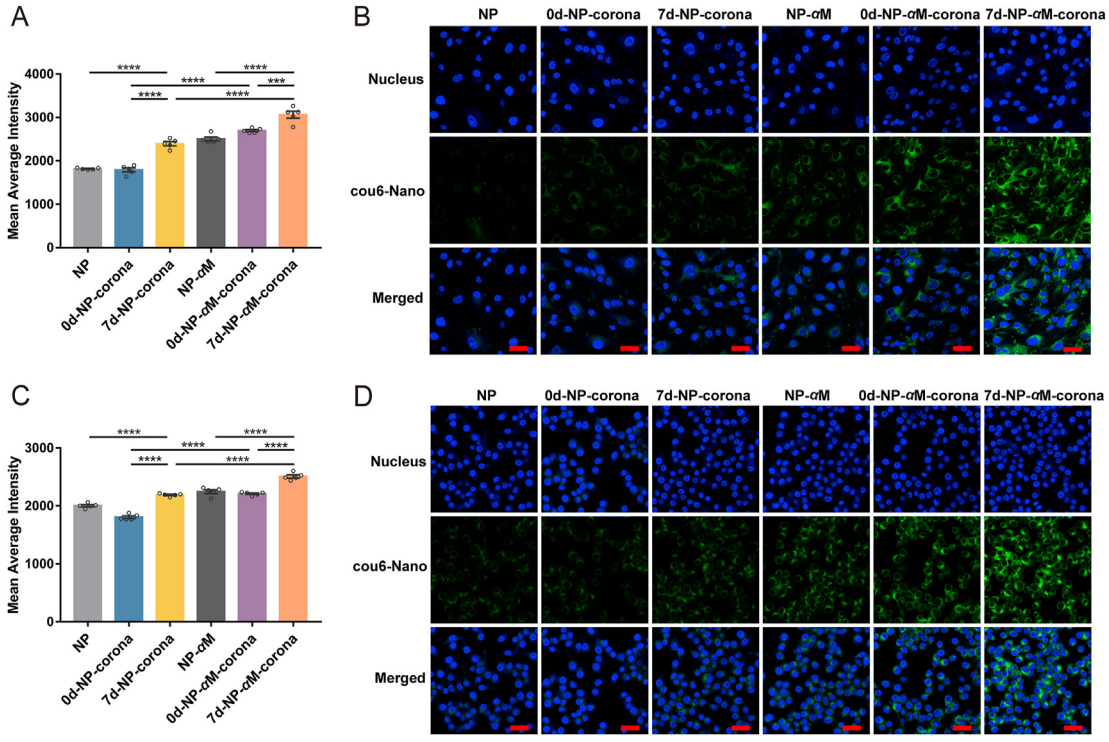

Figure 3 Cellular uptake of NP-corona complexes under different loading and incubation conditions in b.End3 and BV-2 cells. (A and C) Quantitative analysis of NP, NP-αM and NP-corona complexes in b.End3 (A) and BV-2 (C) cells. NP-corona complexes formed on NP or NP-αM in 0d-plasma or 7d-plasma were isolated as described in the Methods. All nanoparticles were labeled with cou6 and incubated with cells for 3 h at the concentration of 15 μg/mL. (B and D) Laser confocal imaging of NP, NP-αM and NP-corona complexes in b.End3 (B) and BV-2 (D) cells, Scale bar = 50 μm. Data are presented as the mean ± SD (n = 5). *P < 0.05, **P < 0.01, ***P < 0.001, ****P < 0.0001.

spectrometry. As shown in the heatmap, nanoparticles with different loading or incubation conditions led to adsorption of different types and amounts of proteins. A significantly higher total number of proteins was detected in the corona formed on nanoparticles loaded with αM (n = 1730 in 7d-NP-αM-corona; n = 1745 in 0d-NP-αM-corona) in comparison with unloaded (n = 986 in 7d-NP-corona; n = 710 in 0d-NP-corona) (Fig. 5A and B). ^{1}H NMR analysis of functional groups on the surface of nanoparticles indicated the existence of the hydrophobic functional group CH_3O– on NP-αM (Figs. S1 and S2), which could contribute to the absorption of a larger number of proteins.

As shown in the Venn diagrams, the levels of 395 proteins were enhanced in 0d-NP-αM-corona compared with 0d-NP-corona, while that of 162 proteins were upregulated in 7d-NP-αM-corona compared with 7d-NP-corona. The intersection of Venn diagrams showed 88 common proteins (Fig. 5C). Top 30 proteins among the 88 common proteins were displayed in the heatmap, among which two proteins associated with endocytosis, CD36 and RAB5A were found (Fig. 5E). RAB5A has been reported to involve in the fusion of plasma membranes and early endosomes[38]. CD36 is related to the phagocytosis of microglia and the lipoprotein endocytosis by endothelial cells[39,40]. Therefore, we hypothesized that RAB5A and CD36 are engaged in the cellular uptake of NP-corona complexes loaded with αM.

Moreover, compared with 0d-NP-corona, 465 proteins were upregulated in 7d-NP-corona, while compared with 0d-NP-αM-corona, 578 proteins were upregulated in 7d-NP-αM-corona (Fig. 5D). Venn diagrams reported 225 common proteins in the intersection (Fig. 5D), among which top 60 proteins were displayed in the heatmap (Fig. 5F). We then performed GO analysis, and found that complement activation and immunoglobulin receptor binding are significantly enriched in both the comparison between 7d-NP-corona and 0d-NP-corona (Fig. 5G and H), and the comparison between 7d-NP-αM-corona and 0d-NP-αM-corona (Fig. 5I and J). It has been reported that complement proteins and immunoglobulins are positive correlated with the phagocytic uptake[41–44]. We hypothesized that the enrichment of complement proteins and immunoglobulins contribute to the enhancement of cellular uptake efficiency of NP-corona complexes formed in 7d-plasma. This hypothesis was consistent with the heatmap in Fig. 5F, in which a number of complement proteins and immunoglobulins were upregulated in the corona of nanoparticles incubated with 7d-plasma compared with 0d-plasma. Meanwhile, immunoglobulin and complement proteins were also found enriched in the 7d-plasma (Supporting Information Table S6), which could be a key cause of the change of protein corona composition.

3.5. Mechanism study of the cellular uptake of NP-corona complexes under different loading and incubation conditions

We continued to determine the potential mechanisms of cellular uptake of the different NP-corona complexes in b.End3 and BV2 cells. Proteomic analysis suggested that the enrichment of complement proteins and immunoglobulins in the corona might promote the cellular uptake efficiency of NP-corona complexes incubated with 7d-plasma. EDTA, a global inhibitor of all complement activation pathways, including classical pathway (CP), lectin pathway (LP) and alternative pathway (AP) was used to

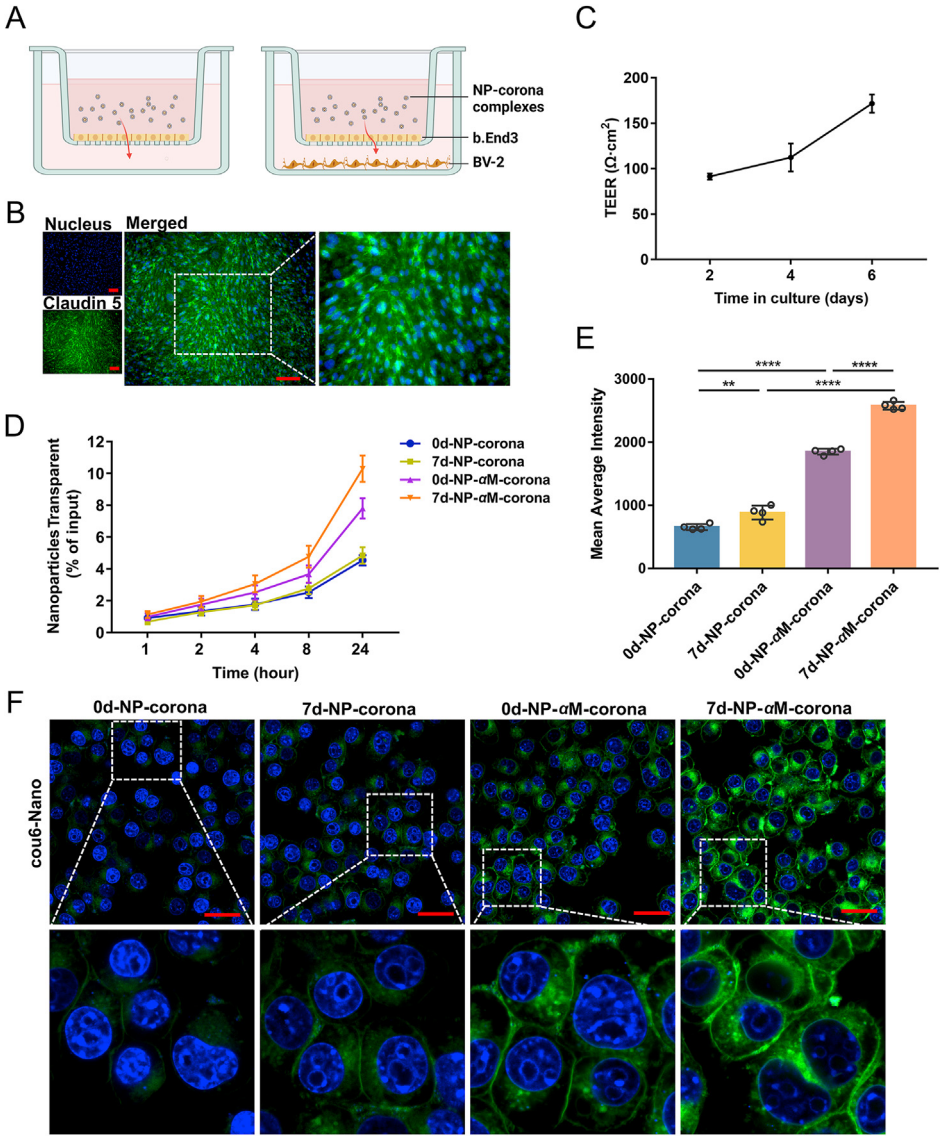

Figure 4 Blood−brain barrier permeability of the NP−corona complexes. (A) Schematic diagram of the *in vitro* BBB-Transwell model. (B) Laser confocal imaging of tight junction protein claudin-5 in the BBB model. Scale bar = 40 μm. (C) The TEER of b.End3 cells were measured at the culture time of 2, 4 and 6 days. (D) The percentage of NP-corona complexes transported across the BBB ($n = 3$). (E and F) Quantitative analysis (E) and laser confocal imaging (F) of the cellular uptake of NP-corona complexes in BV-2 cells cultured at the bottom of the BBB model, in which the nanoparticles firstly crossed the BBB and then got access to the microglia for 12 h, Scale bar = 40 μm. Green: cou6-Nano, Blue: Nucleus. Data are presented as the mean ± SD ($n = 4$). *$P < 0.05$, **$P < 0.01$, ***$P < 0.001$, ****$P < 0.0001$.

evaluate the contribution of complement system[45,46]. It is well-known that the activation of the CP and LP of the complement system is Ca^{2+}-dependent, whereas Mg^{2+} is essential for the operation of the AP[47,48]. The incubation of NPs with plasma was performed in the presence of EDTA to chelate both Ca^{2+} and Mg^{2+}, a previous developed method to inhibit the binding of complement protein to the surface of nanoparticles[45]. Consistent with previous observations, the uptake of NP-corona complexes incubated with 7d-plasma (7d-NP-corona or 7d-NP-αM-corona) was much higher than that with 0d-plasma (0d-NP-corona or 0d-NP-αM-corona) in b.End3 (Fig. 6A and B) and BV-2 cells (Fig. 6C and D). In experiment of EDTA treatment, the uptake of 7d-NP-corona (by 116%) and 7d-NP-αM-corona (by 120%) were significantly reduced in b.End3 cells (Fig. 6A and B). Meanwhile, the uptake of 7d-NP-corona (by 152%) and 7d-NP-αM-corona (by 164%) were suppressed in BV-2 cells (Fig. 6C and D). These results suggest that complement activation is involved in the internalization of NP-corona complexes in both b.End3 and BV-2 cells.

The cellular uptake might also be enhanced by the binding of the exposed Fc regions of immunoglobulins to FcγR on the surface of cells[49]. To test this hypothesis, we pre-incubated the cells with CD16/32 antibody to block the binding of immunoglobulins in the corona to the FcγRIII and FcγRII on the surface of cells. The uptake of 7d-NP-corona (by 96%) and 7d-NP-αM-corona (by 194%) were significantly reduced in b.End3 cells (Fig. 6A and B). While the uptake of 7d-NP-corona and 7d-NP-αM-corona were not suppressed in BV-2 cells (Fig. 6C and D). These results

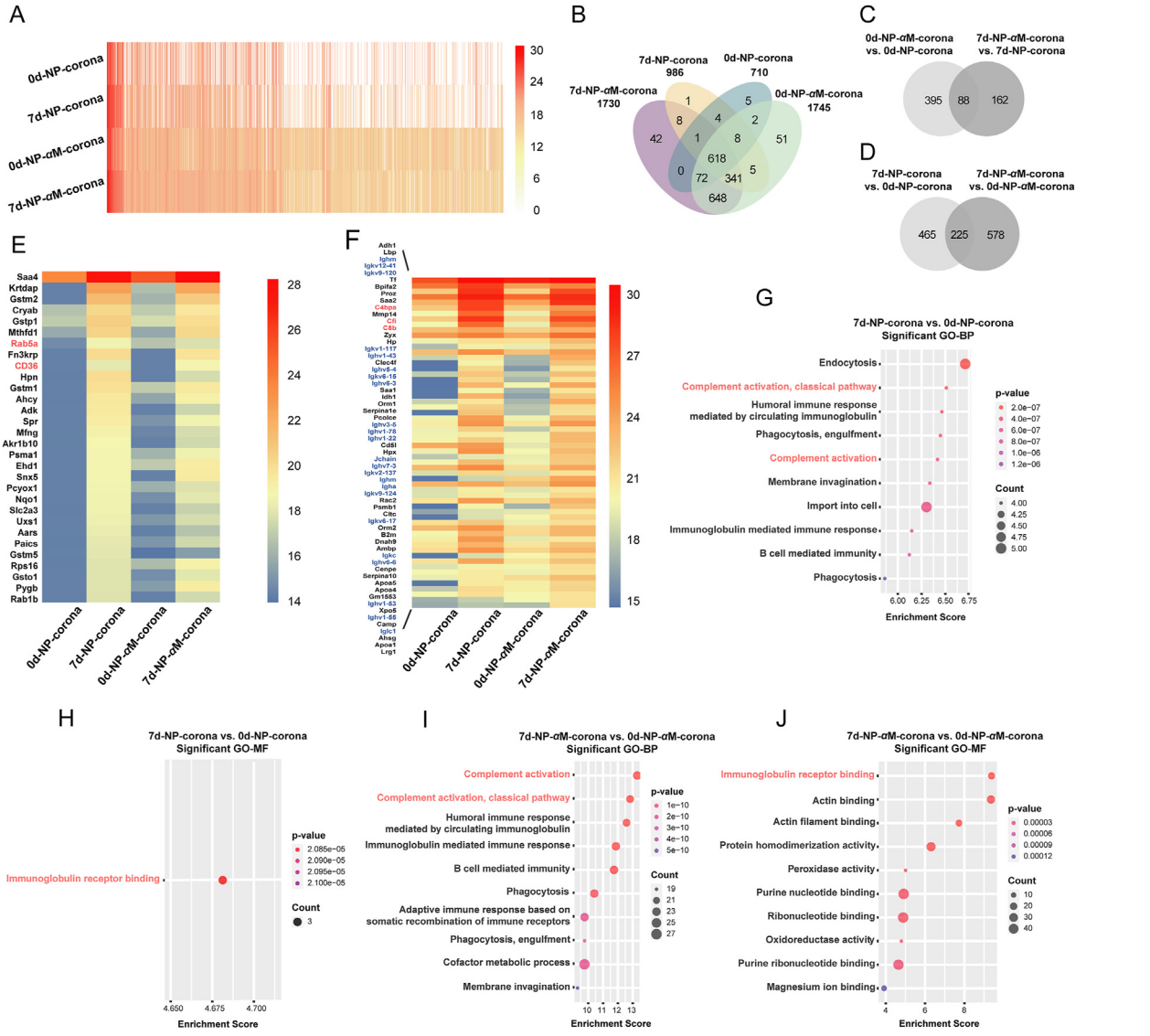

Figure 5 Proteomics analysis of the corona formed on NP or NP-αM in 0d-plasma or 7d-plasma. (A) Heatmap of relative abundance ($\log_2$ scale) values for each corona protein between samples. (B) Venn diagram of the total amount of proteins in NP-corona complexes. (C) The light gray of the Venn diagram indicates the upregulated proteins of 0d-NP-αM-corona compared to 0d-NP-corona, and the dark gray indicates the upregulated proteins of 7d-NP-αM-corona compared to 7d-NP-corona (fold change $>$ 1.5, P value $<$ 0.05). Venn diagram reports the number of unique and common proteins. (D) The light gray of the Venn diagram indicates the upregulated proteins of 7d-NP-corona compared to 0d-NP-corona, and the dark gray indicates the upregulated proteins of 7d-NP-αM-corona compared to 0d-NP-αM-corona (fold change $>$ 1.5). Venn diagram reports the number of unique and common proteins. (E) Heatmap of relative abundance ($\log_2$ scale) values for the top 30 proteins (ordered by maximum fold change) among the common proteins in (C) are displayed. (F) Heatmap of relative abundance ($\log_2$ scale) values for the top 60 proteins (ordered by maximum relative abundance values) among the common proteins in (D) are displayed. (G–J) GO analysis of the upregulated proteins (fold change $>$ 1.5) of 7d-NP-corona compared to 0d-NP-corona (G and H) and 7d-NP-αM-corona compared to 0d-NP-αM-corona (I and J).

indicate that Fcγ receptor-mediate phagocytosis is involved in the internalization of NP-corona complexes in b.End3 cells, not in BV-2 cells.

Proteomic analysis indicated that the enrichment of RAB5A and CD36 in the protein corona might promoted the cellular uptake of NP-corona complexes with αM loading. These proteins might play an important role in enhancing the delivery of NP-αM to the brain and microglia. In order to evaluate the role of RAB5A and CD36 in the uptake of the nanoparticles, we used RAB5A and CD36 antibody to block the specific protein on the surface of NP-corona complexes. The cellular uptake showed a dramatically enhancement in NP-corona complexes loaded with αM (0d-NP-αM-corona or 7d-NP-αM-corona) compared to unloaded (0d-NP-corona or 7d-NP-corona) in b.End3 (Fig. 6E and F) and BV-2 cells (Fig. 6G and H). In the presence of CD36 and RAB5A antibody, nanoparticle uptake was strongly reduced for 0d-NP-αM-corona (by 47% and 43%, respectively) and 7d-NP-αM-corona (by 40% and 46%, respectively) in b.End3 cells (Fig. 6E and F). Similar effects of CD36 and RAB5A antibody in the uptake of 0d-NP-αM-corona (reduced by 73% and 54%,

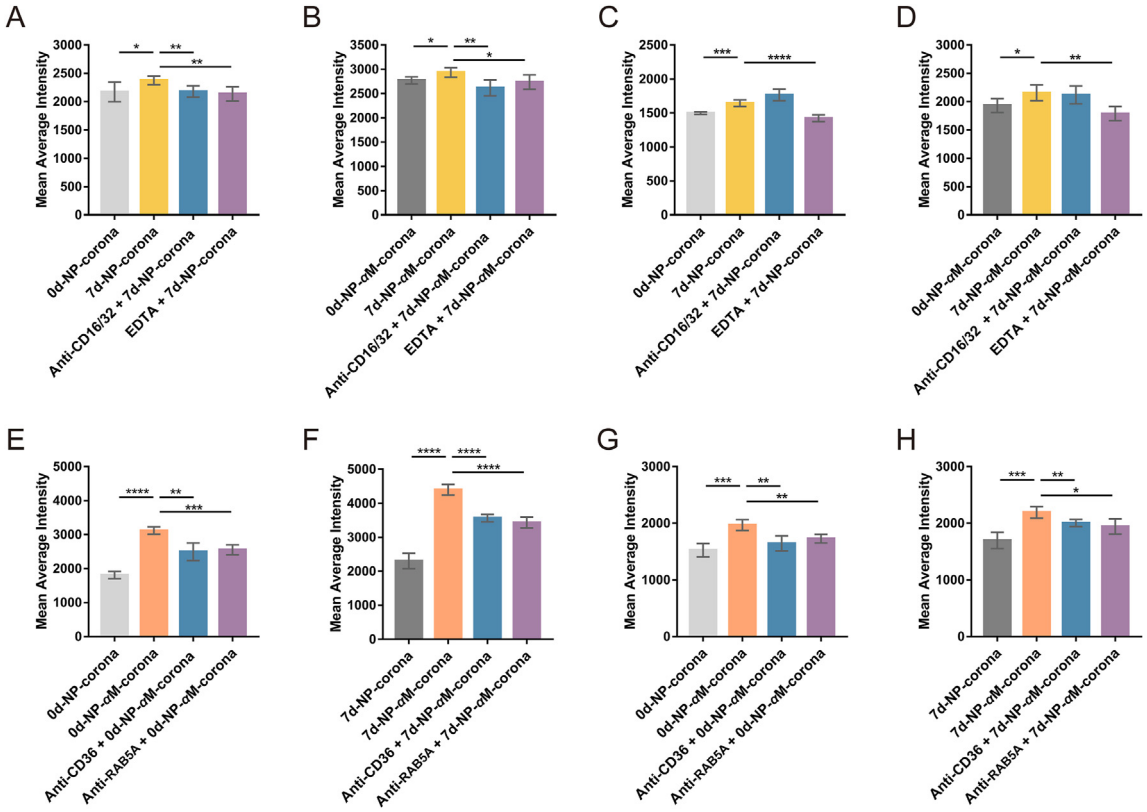

Figure 6 Uptake Mechanisms of NP-corona complexes under different loading and incubation conditions. NP-corona complexes formed on NP or NP-αM in 0d-plasma or 7d-plasma were isolated as described in the Methods. All NP-corona complexes were labeled with cou6 and incubated with cells for 3 h in DMEM at the concentration of 15 μg/mL. (A and C) b.End3 (A) and BV-2 (C) cells were exposed to 7d-NP-corona with or without the treatment of 5 μg/mL anti-CD16/32 or 10 m mol/L EDTA, and 0d-NP-corona as control. (B and D) b.End3 (B) and BV-2 (D) cells were exposed to 7d-NP-αM-corona with or without the treatment of 5 μg/mL anti-CD16/32 or 10 mmol/L EDTA, and 0d-NP-αM-corona as control. (E and G) b.End3 (E) and BV-2 (G) cells were exposed to 0d-NP-αM-corona with or without the treatment of 1 μg/mL anti-CD36 or 1 μg/mL anti-Rab5a, and 0d-NP-corona as control. (F and H) b.End3 (F) and BV-2 (H) cells were exposed to 7d-NP-αM-corona with or without the treatment of 1 μg/mL anti-CD36 or 1 μg/mL anti-Rab5a, and 7d-NP-corona as control. Data are presented as the mean ± SD ($n = 5$). *$P < 0.05$, **$P < 0.01$, ***$P < 0.001$, ****$P < 0.0001$.

respectively) and 7d-NP-αM-corona (reduced by 38% and 37%, respectively) were observed in BV-2 cells (Fig. 6G and H), suggesting that the presence of RAB5A and CD36 in the corona can lead to an increased uptake.

Several studies have shown that disease state (such as tumors) may affect the composition of protein corona and influence the targeting ability of nanoparticles[50,51]. Accordingly, we analyzed and compared the composition of protein corona formed after incubating the nanoparticles with plasma from MCI patients (MCI-NP-αM-corona) and healthy people (Healthy-NP-αM-corona), respectively. CD36 and RAB5A were found in both MCI-NP-αM-corona and Healthy-NP-αM-corona, suggesting that the functional protein absorption could also exist under disease state to enhance the brain distribution of the nanoparticles (Supporting Information Table S7).

4. Discussion

Nanoparticles adsorb a wide range of proteins when enter the biological environment[13]. The formed protein corona provides the nanoparticles with a "biological identity" that affects the pharmacokinetics, biodistribution, cellular association, and targeting ability *in vivo*. In this study, we investigated how the drug-loaded PEG-PLA nanoparticles cross the blood–brain barrier and access microglia, and found that the composition of protein corona on PEG-PLA nanoparticles varied under different drug loading and dosing frequency. These changes of protein corona subsequently affected the cellular uptake of nanoparticles in b.End3 and BV-2 cells with the association of specific adsorbed components, and thereby influenced the brain delivery property and microglia-targeted internalization of nanoparticles *in vivo*.

Microglia are resident immune cells in the central nervous system (CNS). They are critical regulators to maintain homeostasis of the CNS[52]. However, microglia may themselves initiate neural dysfunction and neurodegeneration through loss of homeostatic and/or gain of aberrant function, revealing their potential as therapeutic targets[53]. Unfortunately, drug compounds cannot easily access to microglia due to the obstacle of BBB. It is likely to be important to develop highly-efficient nanoparticulate delivery system that can cross BBB and specifically target microglia.

Recently, several studies have been conducted to develop promising nanoparticles by modulating the composition of formed corona in blood circulation. Guan et al.[54] modified ligand D8 on liposomes to improve immunocompatibility by attenuating natural IgM absorption. Zhang et al.[55] developed SP-sLip to achieve brain-targeted delivery by adsorbing plasma apolipoproteins E, A1 and J on the surface of nanocarriers. Controlling the corona

composition on the surface of nanoparticles could offer exciting possibilities in specific drug delivery. Therefore, a better understanding of the uptake mechanisms of nanoparticles might help engineer more efficacious systems.

Our results indicated that the composition of protein corona formed on PEG-PLA nanoparticles varied under different loading and multiple dosing condition. The specific corona composition we found can affect the cellular uptake and, as a result, nanoparticles can be internalized *via* different mechanisms when adsorbed with different protein coronas. This could subsequently affect the brain delivery and microglia targeting efficiency of nanoparticles.

Many studies have shown that the adsorbed opsonins (such as complement proteins and immunoglobulins) can interact with immune cells *via* membrane receptors and subsequently induce phagocytosis of the nanoparticles[6,45,56]. Despite that PEGylation can reduce the binding of plasma proteins[24], our studies demonstrate that complement proteins and immunoglobulins are enriched in the corona of nanoparticles incubated with 7d-plasma. We found that both complement activation and Fcγ receptor-mediate phagocytosis are involved in the internalization of nanoparticles in b.End3 cells, which may contribute to the process of crossing BBB. Moreover, complement activation is related to the internalization of nanoparticles in BV-2 cells, which may contribute to accessing microglia. However, repeated injection of PEGylated nanopharmaceuticals may also lead to unexpected immune-mediated side effects such as allergic responses, due to anti-PEG antibodies triggered complement activation[6,57]. Thus, a balance between their side effects and the benefit of targeting is necessary to be considered in engineering the nano-surface of drug delivery systems.

Additionally, our results show that RAB5A and CD36 in the corona can enhance the cellular uptake of αM-loaded nanoparticles in both b.End3 and BV-2 cells. RAB5A has been reported to be associated with the fusion of plasma membranes and early endosomes[38]. It is the major regulator of clathrin-mediated endocytosis[58,59], which may be the pathway involved in nanoparticles uptake. CD36 is a kind of integral proteins expressed on the membrane of macrophages, endothelial and microglial cells. It has been reported that CD36 is associated with the recruitment of caveolin and subsequently play the role of phagocytosis[60]. Therefore, the enhancement of nanoparticles uptake in the presence of CD36 may be related to caveolin-mediated endocytosis. Further studies are required to characterize the details of the mechanisms involved in these potential proteins.

It is commonly believed that drug loading hardly influences the biological processing of nanoparticles. However, we found that the brain distribution and cellular uptake of nanoparticles increased significantly after αM loading. Previous studies found that, with the increase of nanoparticles hydrophobicity, more proteins could be adsorbed on the surface[61,62]. Therefore, the increased hydrophobic functional group CH_3O on the surface of NP-αM is very likely contribute to the larger number of protein absorption, in which the enrichment of RAB5A and CD36 might play an important role in enhancing the delivery of NP-αM to the brain and microglia.

Repeated administration also caused the change of protein corona composition. Proteomic analysis showed that although the total number of proteins absorbed on the surface of the nanoparticles hardly changed between the 7d-NP-αM-corona and 0d-NP-αM-corona (and 7d-NP-corona and 0d-NP-corona), the specific protein composition altered. This could be due to the significant differences in plasma protein composition after repeated nanoparticle administration, in which immunoglobulin and complement proteins were found enriched in the 7d-plasma.

Beside dosing frequency and loading condition, other factors likely to influence corona composition should also be taken into consideration, such as PEG density, different routes of administration and disease condition. Moreover, the determination of protein corona formed *in vivo* would better reflect the protein corona on the biological behavior of the nanoparticles. However, the separation of protein corona formed *in vivo* is rather complex, usually need several steps such as centrifugation, size exclusion chromatography separation and ultrafiltration[50,63]. These processes may largely remove the soft corona on the surface of nanoparticles. As proteins in the soft corona also play an important role in the biological process of nanoparticles[64], we prepared the nanoparticle−corona complexes by simple centrifugation immediately after incubating the nanoparticle with fresh plasma. Previous studies showed that with such preparation process, similar major components in corona formed *in vivo* and *in vitro*[55]. The differences in the compositions and biological processing of protein corona formed *in vitro* and *in vivo* need further exploration and more works should be done to optimize purification technology. Dosages may also be an important factor in the protein corona formation. Different dosages may produce different therapeutic effects and change the biofluid environment, which may lead to different protein corona on the nanoparticles. More work is required to fully disentangle the association between the corona and biological fate of nanocarriers.

5. Conclusions

Collectively, here we revealed the influences of drug loading and dosing frequency on the brain delivery property of PEG-PLA nanoparticles, and found that nanoparticles showed higher brain transport efficiency and microglia uptake efficiency after αM loading and multiple administration. We presented an investigation on the corona that formed on NP and NP-αM under various plasma incubation conditions, and linked these coronas to the *in vitro* cellular uptake in b.End3 and BV-2 cells. Our results demonstrate that, both drug loading and multiple dosing have an effect on the resulting corona and subsequent cellular uptake of PEG-PLA nanoparticles. Some components in the corona such as complement proteins, immunoglobulins, RAB5A and CD36 are associated with the process of nanoparticle internalization. Taken together, this suggests, different corona composition can affect the cellular uptake of nanoparticles by different mechanisms, and thereby may influence the brain delivery property of nanoparticles *in vivo*. Our data provide new insights into the development of brain or microglia-specific targeted delivery system.

Acknowledgments

We thank Li Xia from the Core Facility of Basic Medical Sciences of Shanghai Jiao Tong University College for the support in mass spectrometry proteomic analysis. This work was supported by National Natural Science Foundation of China (No. 81722043, 92068111, 81973272, 81803089, 81903582, 82073836), National Science and Technology Major Project (2018ZX09734005, 2017ZX09304016, China), and grant from Shanghai Science and Technology Committee (19410710100, 18YF1413400, China).

Author contributions

Yuyun Tang and Xiaoling Gao designed the research. Yuyun Tang and Jinchao Gao carried out experiments. Tao Wang collected and provided the human plasma samples. Yuyun Tang performed analytical methods, and wrote the manuscript. Qian Zhang, Antian Wang, Meng Huang, Renhe Yu participated part of the experiments. Hongzhuan Chen, Xiaoling Gao interpreted and discussed the data, Xiaoling Gao reviewed and edited the manuscript.

Conflicts of interest

The authors declare no conflict of interest.

Appendix A. Supporting information

Supporting data to this article can be found online at https://doi.org/10.1016/j.apsb.2021.09.029.

References

1. Pardridge WM. Drug transport across the blood–brain barrier. *J Cereb Blood Flow Metab* 2012;**32**:1959–72.
2. Dai TC, Jiang K, Lu WY. Liposomes and lipid disks traverse the BBB and BBTB as intact forms as revealed by two-step Forster resonance energy transfer imaging. *Acta Pharm Sin B* 2018;**8**:261–71.
3. Dong XW. Current strategies for brain drug delivery. *Theranostics* 2018;**8**:1481–93.
4. Zhou YQ, Peng ZL, Seven ES, Leblanc RM. Crossing the blood–brain barrier with nanoparticles. *J Control Release* 2018;**270**:290–303.
5. Gao HL. Progress and perspectives on targeting nanoparticles for brain drug delivery. *Acta Pharm Sin B* 2016;**6**:268–86.
6. Furtado D, Bjornmalm M, Ayton S, Bush AI, Kempe K, Caruso F. Overcoming the blood–brain barrier: the role of nanomaterials in treating neurological diseases. *Adv Mater* 2018;**30**:e1801362.
7. Shin HC, Cho H, Lai TC, Kozak KR, Kolesar JM, Kwon GS. Pharmacokinetic study of 3-in-1 poly(ethylene glycol)-*block*-poly(D,L-lactic acid) micelles carrying paclitaxel, 17-allylamino-17-demethoxygeldanamycin, and rapamycin. *J Control Release* 2012;**163**:93–9.
8. Kim TY, Kim DW, Chung JY, Shin SG, Kim SC, Heo DS, et al. Phase I and pharmacokinetic study of Genexol-PM, a cremophor-free, polymeric micelle-formulated paclitaxel, in patients with advanced malignancies. *Clin Cancer Res* 2004;**10**:3708–16.
9. Gref R, Minamitake Y, Peracchia MT, Trubetskoy V, Torchilin V, Langer R. Biodegradable long-circulating polymeric nanospheres. *Science* 1994;**263**:1600–3.
10. Gao XL, Tao WX, Lu W, Zhang QZ, Zhang Y, Jiang XG, et al. Lectin-conjugated PEG-PLA nanoparticles: preparation and brain delivery after intranasal administration. *Biomaterials* 2006;**27**:3482–90.
11. Olivier JC. Drug transport to brain with targeted nanoparticles. *NeuroRx* 2005;**2**:108–19.
12. Yao L, Gu X, Song QX, Wang XL, Huang M, Hu M, et al. Nano-formulated alpha-mangostin ameliorates Alzheimer's disease neuropathology by elevating LDLR expression and accelerating amyloid-beta clearance. *J Control Release* 2016;**226**:1–14.
13. Monopoli MP, Aberg C, Salvati A, Dawson KA. Biomolecular coronas provide the biological identity of nanosized materials. *Nat Nanotechnol* 2012;**7**:779–86.
14. Nel AE, Madler L, Velegol D, Xia T, Hoek EM, Somasundaran P, et al. Understanding biophysicochemical interactions at the nano-bio interface. *Nat Mater* 2009;**8**:543–57.
15. Lundqvist M, Stigler J, Elia G, Lynch I, Cedervall T, Dawson KA. Nanoparticle size and surface properties determine the protein corona with possible implications for biological impacts. *Proc Natl Acad Sci U S A* 2008;**105**:14265–70.
16. Duan XP, Li YP. Physicochemical characteristics of nanoparticles affect circulation, biodistribution, cellular internalization, and trafficking. *Small* 2013;**9**:1521–32.
17. Mirshafiee V, Kim R, Mahmoudi M, Kraft ML. The importance of selecting a proper biological milieu for protein corona analysis *in vitro*: human plasma *versus* human serum. *Int J Biochem Cell Biol* 2016;**75**:188–95.
18. Moghimi SM, Hunter AC, Andresen TL. Factors controlling nanoparticle pharmacokinetics: an integrated analysis and perspective. *Annu Rev Pharmacol Toxicol* 2012;**52**:481–503.
19. Walkey CD, Chan WC. Understanding and controlling the interaction of nanomaterials with proteins in a physiological environment. *Chem Soc Rev* 2012;**41**:2780–99.
20. Kah JC, Chen J, Zubieta A, Hamad-Schifferli K. Exploiting the protein corona around gold nanorods for loading and triggered release. *ACS Nano* 2012;**6**:6730–40.
21. Wagner S, Zensi A, Wien SL, Tschickardt SE, Maier W, Vogel T, et al. Uptake mechanism of ApoE-modified nanoparticles on brain capillary endothelial cells as a blood–brain barrier model. *PLoS One* 2012;**7**:e32568.
22. Caracciolo G, Cardarelli F, Pozzi D, Salomone F, Maccari G, Bardi G, et al. Selective targeting capability acquired with a protein corona adsorbed on the surface of 1,2-dioleoyl-3-trimethylammonium propane/DNA nanoparticles. *ACS Appl Mater Interfaces* 2013;**5**:13171–9.
23. Caracciolo G, Farokhzad OC, Mahmoudi M. Biological identity of nanoparticles *in vivo*: clinical implications of the protein corona. *Trends Biotechnol* 2017;**35**:257–64.
24. Otsuka H, Nagasaki Y, Kataoka K. PEGylated nanoparticles for biological and pharmaceutical applications. *Adv Drug Deliv Rev* 2003;**55**:403–19.
25. Kim HR, Andrieux K, Delomenie C, Chacun H, Appel M, Desmaele D, et al. Analysis of plasma protein adsorption onto PEGylated nanoparticles by complementary methods: 2-DE, CE and Protein Lab-on-chip system. *Electrophoresis* 2007;**28**:2252–61.
26. Hamad I, Al-Hanbali O, Hunter AC, Rutt KJ, Andresen TL, Moghimi SM. Distinct polymer architecture mediates switching of complement activation pathways at the nanosphere-serum interface: implications for stealth nanoparticle engineering. *ACS Nano* 2010;**4**:6629–38.
27. Ishida T, Harada M, Wang XY, Ichihara M, Irimura K, Kiwada H. Accelerated blood clearance of PEGylated liposomes following preceding liposome injection: effects of lipid dose and PEG surface-density and chain length of the first-dose liposomes. *J Control Release* 2005;**105**:305–17.
28. Yang Q, Lai SK. Anti-PEG immunity: emergence, characteristics, and unaddressed questions. *Wiley Interdiscip Rev Nanomed Nanobiotechnol* 2015;**7**:655–77.
29. Lu W, Wan J, She ZJ, Jiang XG. Brain delivery property and accelerated blood clearance of cationic albumin conjugated pegylated nanoparticle. *J Control Release* 2007;**118**:38–53.
30. Ishihara T, Takeda M, Sakamoto H, Kimoto A, Kobayashi C, Takasaki N, et al. Accelerated blood clearance phenomenon upon repeated injection of PEG-modified PLA-nanoparticles. *Pharm Res* 2009;**26**:2270–9.
31. Jung S, Aliberti J, Graemmel P, Sunshine MJ, Kreutzberg GW, Sher A, et al. Analysis of fractalkine receptor CX_3CR1 function by targeted deletion and green fluorescent protein reporter gene insertion. *Mol Cell Biol* 2000;**20**:4106–14.
32. Tang XL, Liang Y, Zhu YQ, Xie CM, Yao AX, Chen L, et al. Anti-transferrin receptor-modified amphotericin B-loaded PLA-PEG nanoparticles cure Candidal meningitis and reduce drug toxicity. *Int J Nanomedicine* 2015;**10**:6227–41.
33. Wu JZ, Zhao JJ, Zhang B, Qian Y, Gao HL, Yu Y, et al. Polyethylene glycol-polylactic acid nanoparticles modified with cysteine-arginine-

glutamic acid-lysine-alanine fibrin-homing peptide for glioblastoma therapy by enhanced retention effect. *Int J Nanomedicine* 2014;**9**:5261−71.
34. Chen DY, Ganesh S, Wang WM, Amiji M. Plasma protein adsorption and biological identity of systemically administered nanoparticles. *Nanomedicine (Lond)* 2017;**12**:2113−35.
35. Pederzoli F, Tosi G, Vandelli MA, Belletti D, Forni F, Ruozi B. Protein corona and nanoparticles: how can we investigate on? *Wiley Interdiscip Rev Nanomed Nanobiotechnol* 2017;**9**:e1467.
36. Tenzer S, Docter D, Kuharev J, Musyanovych A, Fetz V, Hecht R, et al. Rapid formation of plasma protein corona critically affects nanoparticle pathophysiology. *Nat Nanotechnol* 2013;**8**:772−81.
37. Tehrani SF, Bernard-Patrzynski F, Puscas I, Leclair G, Hildgen P, Roullin VG. Length of surface PEG modulates nanocarrier transcytosis across brain vascular endothelial cells. *Nanomedicine* 2019;**16**:185−94.
38. Kinchen JM, Doukoumetzidis K, Almendinger J, Stergiou L, Tosello-Trampont A, Sifri CD, et al. A pathway for phagosome maturation during engulfment of apoptotic cells. *Nat Cell Biol* 2008;**10**:556−66.
39. Gerbod-Giannone MC, Dallet L, Naudin G, Sahin A, Decossas M, Poussard S, et al. Involvement of caveolin-1 and CD36 in native LDL endocytosis by endothelial cells. *Biochim Biophys Acta Gen Subj* 2019;**1863**:830−8.
40. Dobri AM, Dudau M, Enciu AM, Hinescu ME. CD36 in Alzheimer's disease: an overview of molecular mechanisms and therapeutic targeting. *Neuroscience* 2021;**453**:301−11.
41. Tonigold M, Simon J, Estupinan D, Kokkinopoulou M, Reinholz J, Kintzel U, et al. Pre-adsorption of antibodies enables targeting of nanocarriers despite a biomolecular corona. *Nat Nanotechnol* 2018;**13**:862−9.
42. Quach QH, Kah JC. Non-specific adsorption of complement proteins affects complement activation pathways of gold nanomaterials. *Nanotoxicology* 2017;**11**:382−94.
43. Mahmoudi M, Lynch I, Ejtehadi MR, Monopoli MP, Bombelli FB, Laurent S. Protein–nanoparticle interactions: opportunities and challenges. *Chem Rev* 2011;**111**:5610−37.
44. Simon J, Muller LK, Kokkinopoulou M, Lieberwirth I, Morsbach S, Landfester K, et al. Exploiting the biomolecular corona: pre-coating of nanoparticles enables controlled cellular interactions. *Nanoscale* 2018;**10**:10731−9.
45. Tavano R, Gabrielli L, Lubian E, Fedeli C, Visentin S, Polverino De Laureto P, et al. C1q-mediated complement activation and C3 opsonization trigger recognition of stealth poly(2-methyl-2-oxazoline)-coated silica nanoparticles by human phagocytes. *ACS Nano* 2018;**12**:5834−47.
46. Vu VP, Gifford GB, Chen FF, Benasutti H, Wang GK, Groman EV, et al. Immunoglobulin deposition on biomolecule corona determines complement opsonization efficiency of preclinical and clinical nanoparticles. *Nat Nanotechnol* 2019;**14**:260−8.
47. Merle NS, Church SE, Fremeaux-Bacchi V, Roumenina LT. Complement system part I—molecular mechanisms of activation and regulation. *Front Immunol* 2015;**6**:262.
48. Sahu A, Lambris JD. Structure and biology of complement protein C3, a connecting link between innate and acquired immunity. *Immunol Rev* 2001;**180**:35−48.
49. Pacheco P, White D, Sulchek T. Effects of microparticle size and Fc density on macrophage phagocytosis. *PLoS One* 2013;**8**:e60989.
50. Yu L, Xu MY, Xu WW, Xiao W, Jiang XH, Wang L, et al. Enhanced cancer-targeted drug delivery using precoated nanoparticles. *Nano Lett* 2020;**20**:8903−11.
51. Hadjidemetriou M, Al-Ahmady Z, Buggio M, Swift J, Kostarelos K. A novel scavenging tool for cancer biomarker discovery based on the blood-circulating nanoparticle protein corona. *Biomaterials* 2019;**188**:118−29.
52. Tay TL, Hagemeyer N, Prinz M. The force awakens: insights into the origin and formation of microglia. *Curr Opin Neurobiol* 2016;**39**:30−7.
53. Priller J, Prinz M. Targeting microglia in brain disorders. *Science* 2019;**365**:32−3.
54. Guan J, Shen Q, Zhang Z, Jiang ZX, Yang Y, Lou MQ, et al. Enhanced immunocompatibility of ligand-targeted liposomes by attenuating natural IgM absorption. *Nat Commun* 2018;**9**:2982.
55. Zhang Z, Guan J, Jiang ZX, Yang Y, Liu JC, Hua W, et al. Brain-targeted drug delivery by manipulating protein corona functions. *Nat Commun* 2019;**10**:3561.
56. Weiss ACG, Kelly HG, Faria M, Besford QA, Wheatley AK, Ang CS, et al. Link between low-fouling and stealth: a whole blood biomolecular corona and cellular association analysis on nanoengineered particles. *ACS Nano* 2019;**13**:4980−91.
57. Chen FF, Wang GK, Griffin JI, Brenneman B, Banda NK, Holers VM, et al. Complement proteins bind to nanoparticle protein corona and undergo dynamic exchange *in vivo*. *Nat Nanotechnol* 2017;**12**:387−93.
58. Seachrist JL, Laporte SA, Dale LB, Babwah AV, Caron MG, Anborgh PH, et al. RAB5 association with the angiotensin II type 1A receptor promotes RAB5 GTP binding and vesicular fusion. *J Biol Chem* 2002;**277**:679−85.
59. McLauchlan H, Newell J, Morrice N, Osborne A, West M, Smythe E. A novel role for RAB5-GDI in ligand sequestration into clathrin-coated pits. *Curr Biol* 1998;**8**:34−45.
60. Glatz JF, Luiken JJ, Bonen A. Membrane fatty acid transporters as regulators of lipid metabolism: implications for metabolic disease. *Physiol Rev* 2010;**90**:367−417.
61. Aggarwal P, Hall JB, McLeland CB, Dobrovolskaia MA, McNeil SE. Nanoparticle interaction with plasma proteins as it relates to particle biodistribution, biocompatibility and therapeutic efficacy. *Adv Drug Deliv Rev* 2009;**61**:428−37.
62. Yu QH, Zhao LX, Guo CC, Yan B, Su GX. Regulating protein corona formation and dynamic protein exchange by controlling nanoparticle hydrophobicity. *Front Bioeng Biotechnol* 2020;**8**:210.
63. Al-Ahmady ZS, Hadjidemetriou M, Gubbins J, Kostarelos K. Formation of protein corona *in vivo* affects drug release from temperature-sensitive liposomes. *J Control Release* 2018;**276**:157−67.
64. Schottler S, Becker G, Winzen S, Steinbach T, Mohr K, Landfester K, et al. Protein adsorption is required for stealth effect of poly(ethylene glycol)- and poly(phosphoester)-coated nanocarriers. *Nat Nanotechnol* 2016;**11**:372−7.